Structure Development during Crystallization of Homogeneous Copolymers of Ethene and 1-Octene: Time-Resolved Synchrotron X-ray and SALS Measurements

Y. Akpalu,[†] L. Kielhorn,[†] B. S. Hsiao,[‡] R. S. Stein,*[,†] T. P. Russell,[†] J. van Egmond,[§] and M. Muthukumar*[,†]

Department of Polymer Science and Engineering, University of Massachusetts, Amherst, Massachusetts, 01003, Department of Chemistry, State University of New York at Stony Brook, Stony Brook, New York 11794−3400, and Department of Chemical Engineering, University of Massachusetts, Amherst, Massachusetts, 01003

Received June 26, 1998

ABSTRACT: Crystallization kinetics in a homogeneous copolymer of ethene and 1-octene with appended long chain branches has been investigated in real time by means of time-resolved light scattering under H_V (cross-polarized) and V_V (parallel-polarized) optical alignments using a CCD camera system, simultaneous small angle-X-ray and wide angle X-ray measurements using synchrotron radiation and differential scanning calorimetry (DSC). The data show that in the case of crystallization at large supercooling, a significant fraction of the crystallinity develops after the spherulites have become volume filling. The fraction of crystallinity that develops after primary crystallization increases with crystallization temperature. This opens up a challenge to explore the extent to which this behavior is universal in other crystallizable ethylene copolymers as well.

Introduction

Time-resolved scattering studies on polyethylene[1−8] show that the crystallization of polyethylene from the melt state can be described by two stages: (1) primary crystallization with the growth of superstructures such as spherulites and (2) secondary crystallization during which the degree of crystallinity within the morphological units increases. Although a distinction between primary and secondary crystallization can be made, usually the two processes cannot be completely separated. However, by comparing the time evolution of the degree of crystallinity obtained from wide-angle X-ray scattering (WAXS), the total scattering power obtained from small-angle X-ray scattering (SAXS), and small-angle light scattering (SALS) patterns, it may be possible to identify and separate the crystallization mechanisms in the samples under study. The time evolution of larger scale structures such as spherulites along with that of the lamellae and unit cell can be monitored by simultaneous measurements.[2] The problem with this approach is that the quality of the light scattering patterns obtained are poorer than those obtained by a separate measurement; optimizing the sample cell design for all three measurements compromises the resolution of each individual measurement necessary because the optimal thickness for SALS is much smaller than the one for SAXS or WAXS. The primary disadvantage of performing separate SALS measurements with simultaneous SAXS/WAXS is that, in order to compare the results, one has to match the thermal history of the sample for the different experiments and perform repeated experiments on samples with varying thicknesses.

In this paper, we report the results of our time-resolved simultaneous synchrotron SAXS/WAXS, separate real-time SALS and differential scanning calorimetry (DSC) studies during crystallization of a high density homogeneous copolymer of ethylene and 1-octene (E1) containing long chain branches. This sample belongs to the class of homogeneous ethylene/α-olefins copolymers with appended long chain branches introduced by Dow Chemical Co. in 1992. Previous melt-crystallization studies by Bassett and Hodge[9−12] of various linear polyethylenes with broad and narrow molecular weight distributions have shown that fractionation during crystal growth tends to place different molecular lengths in specific sites within the spherulites. They show that the thin lamellae (and hence the low melting population of the sample) are located between the dominant sheets of the more linear components which have higher melting points and hence crystallize more rapidly. In contrast, the sample studied here is not a mixture of linear and branched polyethylene, the branch distribution between chains is narrow whereas the sequence distribution along the chains is broad.[13] In this sample, we expect that the regions of the chain with longer ethylene sequences will require short times to crystallize than regions with shorter sequences at the same temperature. Our SALS, DSC, and SAXS/WAXS data suggest that the increase in crystallinity observed after spherulitic impingement can be attributed to the crystallization of the shorter ethylene sequences. Our results for the sample studied are new since no real-time scattering studies during crystallization have been reported for a high density polyethylene with appended long chain branches and narrow molecular weight distribution.

Experimental Section

A Type IV ethylene-octene copolymer (E1) synthesized by the Dow INSITE technology[14] and characterized by Dow Chemical Co. was used in this study. E1 has a weight average molecular weight (M_w) of 69 000, a polydispersity (M_w/M_n) of 2.33 and a density of 0.935 g/cm^3. The mole percent octene is 0.21 (0.82 wt%). From our ^{13}C NMR measurements, the number of methyls per 1000 carbon atoms for E1 is about 2,

[†] Department of Polymer Science and Engineering, University of Massachusetts.
[‡] University of New York at Stony Brook.
[§] Department of Chemical Engineering, University of Massachusetts.

10.1021/ma9810114 CCC: $18.00
Published on Web 01/22/1999

and this value is in agreement with the value of 1.82 methyls per 1000 carbon atoms obtained by Dow Chemical Company. The sample contains about one short chain branch and a long chain branch per 1000 carbon atoms that is slightly less than or equal to one as deduced by combining the short chain branching obtained from the feedstock composition with the total branching obtained from NMR and IR results. Our estimate for the number of long chain branch points is consistent with what has been reported.[15] On the basis of the mole percent branch points from ^{13}C NMR, the equilibrium melting point of the sample is about 140 °C.

Melting temperature−composition relations have been established for random copolymers of ethylene with butene, hexene and octene at a fixed molecular weight of 90 000 ± 30 000.[16] The melting temperature of a rapidly quenched sample at a given co-unit content was found to be the same irrespective of either the chemical nature of the branch or the polymerization method. For a random ethylene-1-octene copolymer with 0.21 mol% comonomer, the melting point of a rapidly quenched sample is 123 °C. The melting temperature of our sample under similar conditions is about 123 °C. Small amounts of long chain branches (LCB) in homogeneous poly(ethylene/α-olefins) copolymers has been shown[15] to have little effect on the density and melting peak with compared to samples without LCB. Moreover, type IV ethylene−octene copolymers exhibit a lamellar morphology with well-developed spherulitic superstructure similar to that of high density polyethylene.[14] Although the branches restrict crystallization to some extent, the ethylene sequences are long enough to crystallize in lamellae.[15]

Films with thicknesses ranging from 100 μm to 1 mm were prepared as described previously[6]. For thicknesses less than 100 μm, films were prepared by solvent casting polymer/xylene solutions onto clean glass cover slides. A 2 wt% solution gives films approximately 10 μm thick. For all isothermal crystallization experiments (DSC, SALS, and WAXS), E1 was melted at 160 °C and held at this temperature for 30 minutes before quenching to the desired crystallization temperature. The quenching process for SALS and SAXS/WAXS were carried out by rapidly transferring the sample from a chamber at 160 °C to one at the crystallization temperature while for DSC quenching was achieved with the use of liquid nitrogen. Since different sample chambers were used for X-ray and SALS, the quenching rate differs in the three cases. Unless stated otherwise, all references to time in the following discussion will be made with respect to the time elapsed after the start of quench. DSC experiments were performed on a Perkin-Elmer DSC 7. Temperature and enthalpy values were calibrated using indium as a standard. Measurements were made on 5−10 mg melt-pressed samples sealed in aluminum pans. For this weight range, variations in the heat of crystallization and melting were on the order of 2 J/g. Melting curves were obtained by heating samples past the melting point at 10 °C/min after crystallizing for a specific duration of time.

In order to determine the crystallinity for comparison with WAXS, samples were then heated from the crystallization temperature past the melting point at 10 °C/min after crystallizing for one hour. The apparent degree of crystallinity (w_c^{DSC}) is estimated using $w_c^{DSC} = \Delta H_f/\Delta H°$, where ΔH_f is the heat of fusion obtained by integrating the area under the normalized melting peak and $\Delta H° = 293$ J g^{-1} is the reference heat of fusion for 100% crystalline polyethylene.[17] For rapidly quenched samples, i.e., where thermal equilibration was attained within 60 s after quenching, w_c^{DSC} is 0.38, 0.37 and 0.36 at 114, 114.5 and 115 °C respectively. Within this temperature range, variations in the overall crystallinity are within the uncertainties in measurement. During crystallization, the fraction of crystalline material transformed (X_t^{DSC}) is estimated from the normalized crystallization exotherms by $X_t^{DSC} = \Delta H(t)/\Delta H(\infty)$. Between 114 and 115 °C, the average value of $\Delta H(\infty)$ is 83 J/g.

Time-resolved simultaneous SAXS and WAXS experiments were performed on beam line X3A2 at the National Synchrotron Light Source (NSLS), Brookhaven National Laboratory (BNL). The radiation spectrum from the source was monochromated using a silicon crystal to give an intense X-ray beam at $\lambda = 1.54$ Å. Two linear position detectors controlled by dual multichannel analyzer interface modules were used to collect the SAXS and WAXS data simultaneously. Details of the setup have been described in Hsiao et al.[18] For SAXS, the sample to detector distance was about 920 mm, covering a scattering vector **q** from 0.01 to 0.2 Å^{-1}. The scattering vector is defined as $q = (4\pi/\lambda)\sin(\theta)$ and 2θ is the scattering angle. An evacuated flight path was used in conjunction with the detector. The SAXS patterns were corrected for blank scattering, sample thickness and absorption.[19] The angular range (2θ) WAXS was from 16 to 32° (1.135 Å^{-1} < q < 2.25 Å^{-1}). The accuracy of the temperature in each chamber of the dual-chambered temperature jump cell was ±0.5 °C. The SAXS invariant (Q_{SAXS}) is obtained after correcting the intensities for thermal background (I_b), and extrapolation to $q = 0$ and $q = \infty$. These corrections are performed by applying algorithms developed by Zachmann[22] and Hsiao et al.[23,24] In this algorithm, parameters are estimated by minimizing the total area under the interference function (Fourier transform of the interface distribution function) and that for the Porod region. I_b is modeled[25] as a polynomial of even powers of q. Extrapolation to low q was performed using an intensity profile based on Guinier's law.[26] The long period, L_B is determined by applying Bragg's Law to the peak position of the Iq^2 curve.

The apparent crystallinity from WAXS (w_c^{WAXS}) was calculated as the ratio of the total area under the resolved crystalline peaks to the total area under the unresolved normalized X-ray scattering curve.[19] The resolved area under the crystalline peaks was obtained by drawing baselines under the (110) reflection between 2θ of 20.5 and 22.5° and the (200) reflection between 22.5 and 25.0°. The crystallinity is referred to as "apparent" since corrections associated with the crystal disorder as discussed by Ruland[20,21] were not applied. In order to perform these corrections, one needs to obtain data at larger angles. The unit cell volume and lattice parameters were calculated by assuming that the length of the unit cell in the c-direction, i.e., the molecular chain direction, has a constant value of 2.547 Å, and the mass density of the crystalline phase was obtained by assuming that the unit cell contains four CH_2 groups.[19]

SALS patterns in the H_V and V_V polarization modes were recorded using a vertical SALS apparatus which consists of a He/Ne laser light source ($\lambda = 633$ nm), a polarizer, an analyzer and a CCD camera as the detector. In this setup, the scattering images are collected simultaneously with the incident intensity transmitted through the sample. The H_V and V_V patterns were corrected for distortions of the image arising from the relative orientation of the camera. A more detailed description of the SALS apparatus has been given by Van Egmond and Fuller.[27] A two-temperature chamber device developed in our laboratory was used to approximate the isothermal crystallization conditions used to obtain the synchrotron X-ray data. Films 10−100 μm thick sealed between two cover slides were heated to 160 °C and annealed at this temperature for 30 minutes. During crystallization, temperature changes within the sample, the transmitted intensity and changes in the scattering profiles for each polarization mode were monitored simultaneously. The actual sample temperature was monitored by a thermocouple inserted into the sample cell and the temperature was recorded every second. All temperature and scattering data were stored for later analysis. The H_V and V_V scattering intensities were corrected for sample volume, reflection, and refraction, and the melt contribution is subtracted out after accounting for statistical fluctuations.[28] The integrated intensity calculated represents changes during crystallization or melting and will be referred to as a relative invariant. The spherulite size[29] was estimated from the H_V data.

Results and Discussion

Our real-time SALS results in the temperature range 114−118 °C show that the volume fraction of crystals within the spherulite increases significantly after the spherulites have become volume filling. To discuss the crystallization kinetics from SALS, it is convenient to employ the total integrated scattered intensity (invari-

ant) defined, as with X-ray scattering as $Q = \int_0^\infty I(q)q^2 \, dq$. The H_V pattern obtained for crystallized E1 is characteristic of spherulites. For this morphology, the H_V invariant (Q_{H_V}) is proportional to the mean square anisotropy within the spherulites, $\langle\delta^2\rangle$, while the V_V invariant (Q_{V_V}) depends on both $\langle\delta^2\rangle$ and the mean optical polarizability from the average value, $\langle\eta^2\rangle$.

For spherulites with no internal disorder embedded in an isotropic matrix of amorphous polymer, Q_{H_V} is given by[30,31]

$$Q_{H_v} = \frac{K}{15}\langle\delta^2\rangle \tag{1}$$

$$\langle\delta^2\rangle = x_{sp}(\alpha_r - \alpha_t)_{sp}^{\ 2} \tag{2}$$

$$(\alpha_r - \alpha_t)_{sp} = \delta^o_{cr} x_{cr,s} P_2 + (\alpha_r - \alpha_t)_{am} + \delta_P \tag{3}$$

In eq 3, δ^o_{cr} is the intrinsic anisotropy of a pure crystal, $x_{cr,s}$ is the volume fraction crystallinity within the spherulite and P_2 is a Hermans-type orientation function describing the orientation of the crystals with respect to the radius of the spherulite. The radial and tangential polarizabilities are α_r and α_t, respectively, and K is a product of physical constants. The term $(\alpha_r - \alpha_t)_{am}$ is the amorphous contribution to the spherulite polarization anisotropy, which is assumed to be small. The form anisotropy arising from the effect of the crystal−amorphous boundary on the internal field is δ_P which is assumed to be negligible. When spherulites become volume filling at $x_{sp} = 1$

$$Q_{H_V} = \frac{K}{15}(\delta^o_{cr}\Phi_c^{SALS} P_2)^2 \tag{4}$$

$$\Phi_c^{SALS} = x_{cr,s} \tag{5}$$

where Φ_c^{SALS} is the volume fraction crystallinity which could be obtained from SALS provided that P_2 is known. The corresponding Q_{V_V} is given by[30]

$$Q_{V_V} = K\left\{\cos^2\rho_1\left[\langle\eta^2\rangle + \langle\delta^2\rangle\left(\frac{1}{5} - \frac{x_{sp}}{9}\right)\right] + \sin^2\rho_1\frac{\langle\delta^2\rangle}{15}\right\} \tag{6}$$

$$\langle\eta^2\rangle = x_{sp}(1 - x_{sp})(\bar{\alpha}_{sp} - \alpha_o)(\alpha_t - \alpha_o) \tag{7}$$

$$\bar{\alpha}_{sp} = \frac{\alpha_r + 2\alpha_t}{3} \tag{8}$$

where $\cos^2\rho_1$ and $\sin^2\rho_1$ are geometric correction terms,[30] $\bar{\alpha}_{sp}$ is the average polarizability of the spherulite, and that of the matrix is α_o.

Equations 1−8 describe scattering during the growth of a complete spherulite. During crystallization, the H_V invariant should increase linearly with x_{sp} and as the square of $x_{cr,s}$. The V_V invariant will increase at first reaching a maximum near $x_{sp} = 0.5$ if the polarizability of the matrix is much less than the average polarizability of the spherulite. This is usually true for crystalline polymers. Beyond $x_{sp} = 0.5$, the contribution of $\langle\eta^2\rangle$ decreases, reaching zero, and the V_V invariant goes to a minimum value when the spherulites become volume filling ($x_{sp} = 1$), since the terms arising from the effect of the surrounding polarizabilities go to zero. After spherulitic impingement, any increase in both invariants is a further indication of an increase in the fraction of crystals within the spherulites or their degree of perfection or orientation (P_2 could increase to a limiting value of 1) during secondary crystallization. The second increase in the V_V intensity should be small since for small angles the $\sin^2\rho_1$ term in eq 6 can be ignored, and when $x_{sp} = 1$, $Q_{V_V} = {}^4/_3 Q_{H_V}$.

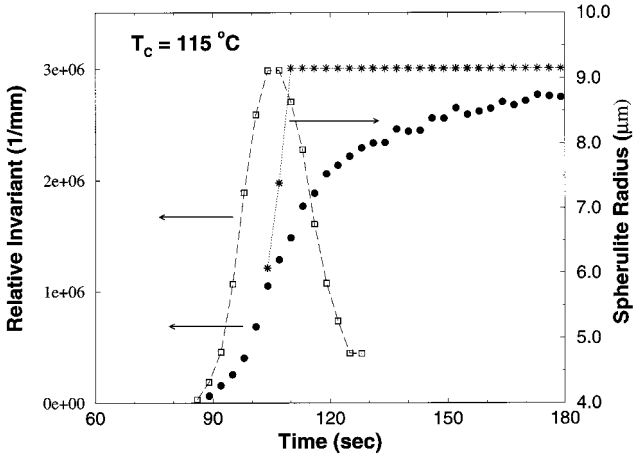

Figure 1. Changes in the relative invariant: (□) V_V, (●) H_V, and the average spherulite radius (∗) during crystallization of E1 at 115 °C.

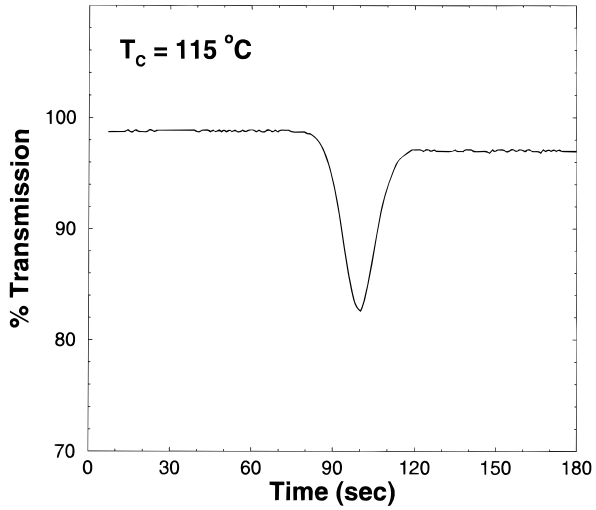

Figure 2. Changes in the percent transmission during crystallization of E1 at 115 °C.

Figure 1 shows the changes in the relative H_V and V_V invariants and the spherulite radius (R_{sp}) during the crystallization of a 22 μm film of E1 at 115 °C. The corresponding transmitted intensity measured simultaneously with the scattering intensity is shown in Figure 2. In the temperature range studied, we find the onset of changes in the H_V and V_V intensities to occur simultaneously. At 115 and 118 °C, our SALS H_V patterns show that during the growth of crystalline aggregates, the shape of the scattering patterns evolve from one with very little azimuthal dependence to one characteristic of mature spherulites. Representative data at 115 °C are shown in Figure 3. This observation indicates that during the early stages of growth, the anisotropy of the growing crystal aggregate is low suggesting a low crystallinity within the spherulites and/or a low degree of orientational correlations of the constituent crystals. At 115 °C, we observe that the percent transmission goes through a minimum while the relative V_V invariant reaches a maximum near 104

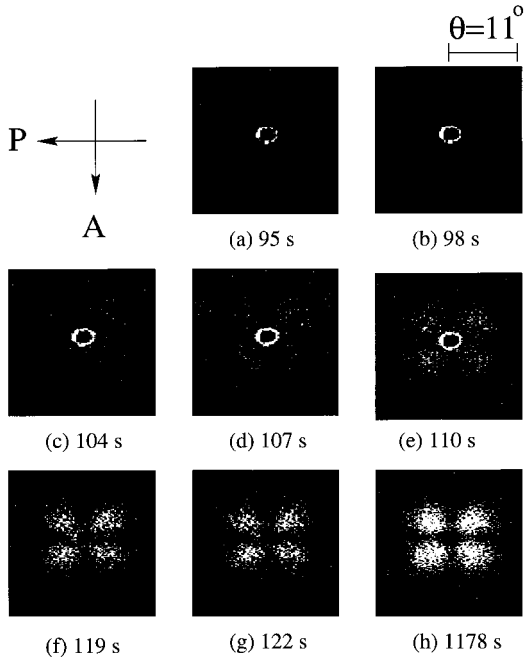

Figure 3. H_V patterns during crystallization of E1 at 115 °C. Melt background contribution has been subtracted.

s. For the percent transmission observed in the region of the maximum V_V invariant, multiple scattering should be largest.[32,33] After 119 ± 1 s, the transmission reaches an asymptotic value while the spherulite radius attains its limiting value of 9.2 μm at 110 s at which time the spherulites become volume filling.

According to eqs 6−8, the V_V invariant must go through a minimum when the spherulites become volume filling and the corresponding pattern should develop a 2-fold symmetry. However at this stage (110 s), the V_V intensity is large as a result of additional density fluctuations contributing to the V_V scattering. This contribution arises from the increasing average refractive index difference between crystalline domains (rich in the most linear sequences) and the molten phase (with more branched sequences), which gives rise to the enhanced density fluctuations within the spherulites. As these branched sequences crystallize, the V_V intensity decreases and the H_V pattern evolves into one characteristic of a mature spherulite; the intensity maximum at small angles arising from these internal density fluctuations decreases and one at larger angles characterizing the size of the spherulites increases (Figures 3). The large increase observed in the H_V invariant after spherulitic impingement strongly suggests that a significant fraction of the material continues to crystallize during this stage.

After spherulitic impingement, the crystallinity within the spherulites is proportional to the square root of the SALS H_V invariant (eq 4). In the absence of absolute measurements, we apply eq 4 to calculate the fraction of crystalline material transformed, $X(t)^{SALS}$, which is given by

$$X(t)^{SALS} = \sqrt{\frac{Q_{H_V}(t)}{Q_{H_V}(\infty)}} \tag{9}$$

Here we have assumed that P_2 does not change significantly after spherulitic impingement. At 115 °C, $X(t)^{SALS}$ is about 70% when the spherulites become volume filling at 110 s and the remaining 30% develops after this stage as a secondary crystallization process. $X(t)^{SALS}$ is about 50% at the end of the primary process (258 s) at 118 °C, and the average spherulite radius is slightly smaller than that attained at 115 °C (Figure 4).

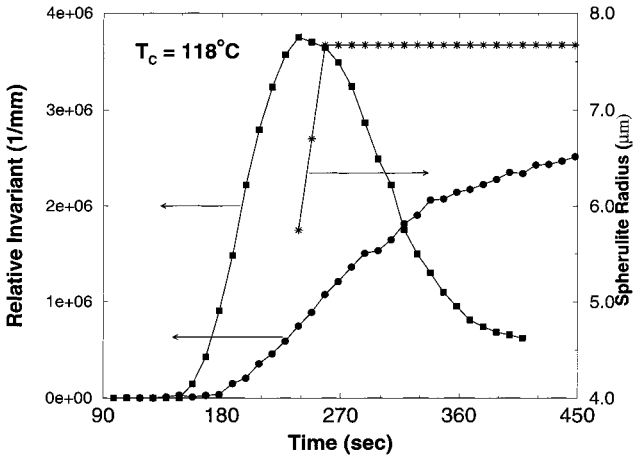

Figure 4. Changes in the relative invariant: (□) V_V, (●) H_V, and the average spherulite radius (∗) during crystallization of E1 at 118 °C.

The SAXS invariant (Q_{SAXS}) for a system where all the crystallizable units are within spherulites is given by[3,22]

$$Q_{SAXS} = C\, x_{sp}\, x_{CL}(1 - x_{CL})(\Delta\rho)^2 \tag{10}$$

In eq 10, C is a factor dependent on geometry and other quantities kept constant during the experiment, $\Delta\rho$ is the electron density difference between the crystalline and amorphous phases, x_{sp} is the volume fraction of polymer transformed into spherulites and x_{CL} is the fraction of crystals within the spherulites. The crystallinity index measured by WAXS (w_c) is the total weight fraction of crystals within the sample which is related to the above quantities by

$$w_c = \left(\frac{\rho_c}{\rho_s}\right)\Phi c \tag{11}$$

$$\Phi_c = x_{sp} x_{CL} \tag{12}$$

$$\rho_s = \rho_c \Phi_c + \rho_a(1 - \Phi_c) \tag{13}$$

where Φ_c is the volume crystallinity which can be estimated from WAXS or from a combination of SAXS and SALS. The electron densities of the crystalline and amorphous regions are designated by ρ_c and ρ_a and that of the sample is ρ_s. The factor (ρ_c/ρ_s) is included to convert volume fractions to weight fractions. The implicit assumption of this model is that all the crystals are in lamellar stacks and there are only two phases (crystalline and amorphous). According to this model, x_{sp} increases from 0 to 1 during primary crystallization. During the primary crystallization of most polymers, the change of x_{CL} is small as compared to the variation in x_{sp} so that x_{CL} can be considered to be almost constant. As a result, Q_{SAXS} and w_c or Φ_c are proportional to x_{sp} (eqs 10 and 12). In contrast, during secondary crystallization, Q_{SAXS} is proportional to $x_{CL}(1 - x_{CL})$ while w_c is proportional to x_{CL}. Thus, for this model during secondary crystallization, the change in w_c will be larger than

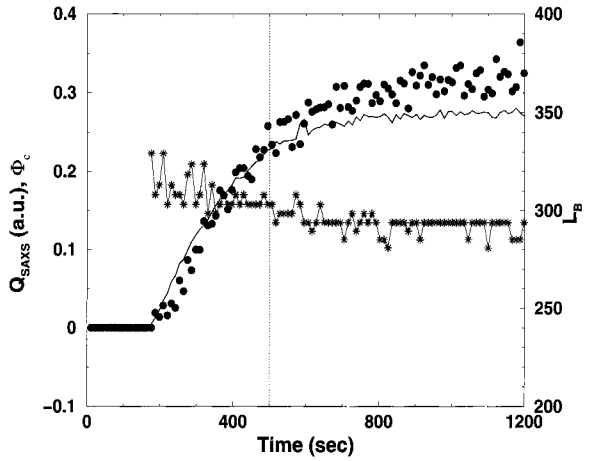

Figure 5. Changes in morphological quantities for synchrotron SAXS/WAXS during crystallization of E1 at an average temperature of 114.5 ± 0.5 °C: volume degree of crystallinity determined from WAXS Φ_c (●), SAXS invariant Q_{SAXS} (—), and the long period L_B from the Iq^2 curve.

the change of Q_{SAXS}, while during primary crystallization Q_{SAXS} and w_c will be proportional to each other.

The SAXS invariant, volume crystallinity from WAXS (Φ_c) and the long period as a function of crystallization time at an average temperature of 114.5 °C are shown in Figure 5. Initially, Q_{SAXS} and Φ_c increase in a similar way. After this initial sharp increase, Q_{SAXS} becomes constant while Φ_c increases at protracted rate. In this case, primary crystallization ends when the fraction of crystalline material transformed ($X(t)^{WAXS} = \Phi_c(t)/\Phi_c(\infty)$) is between 65 and 72% i.e., 500−600 s, $\Phi_c(\infty) = 0.34$ and the average long period is 309 ± 8 Å (dotted line in Figure 5). During the entire process, the long period decreases slightly to the level of 294 ± 5 Å. Such a decrease (in the long period) indicates that the process of primary crystallization produces a lamellar structure which contracts with time.

At this juncture, one may consider alternate two-phase models that can describe the observations. In general, for a two-phase system $Q_{SAXS} = \Phi_c (1 - \Phi_c)(\Delta\rho)^2$. For this model, the curves representing Q_{SAXS} and Φ_c should not be superimposable when Φ_c is larger than 0.15. This expectation is contrary to what we observe (Figure 5). From DSC, we observe a break in the time dependence of the crystallization isotherms at about 68−72% and 52−58% conversion at 115 and 118 °C respectively (Figure 6). The significance of this break has been attributed to the continuation of a secondary process which predominates at the end of primary crystallization.[37] Thus, even though different sample thicknesses and experimental setups were used for our synchrotron X-ray, DSC and SALS measurements, we obtain good agreement for the end of the primary process as a function of the fraction of material transformed to crystals when spherulites become volume filling in all experiments.

The analysis of our synchrotron WAXS data show that during initial stages of primary crystallization, the unit cell lattice parameters contract, the crystal density increases, and the full width at half maximum (fwhm) decreases (Figures 7 and 8). This is consistent with the observation of decrease in the long period observed through SAXS. Crystallization theories have demonstrated that the initial formation of lamellar crystals is kinetically controlled; the observed lamellar thickness is one which grows fastest and is not necessarily the most stable crystal which could have been grown. Thus our observations are consistent with an increase in the perfection of the first formed crystals via the removal of defects.

To discuss the secondary crystallization process after spherulitic impingement, one needs to consider SAXS data obtained simultaneously with WAXS and separate

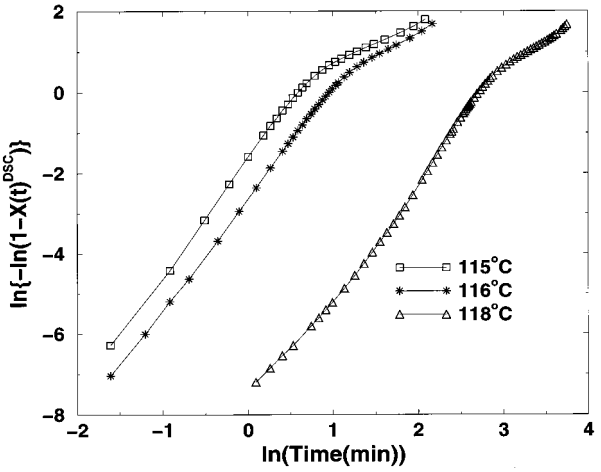

Figure 6. Avrami[34] plots of $X(t)^{DSC}$ during crystallization at (□) 115, (∗) 116, and (△) 118 °C.

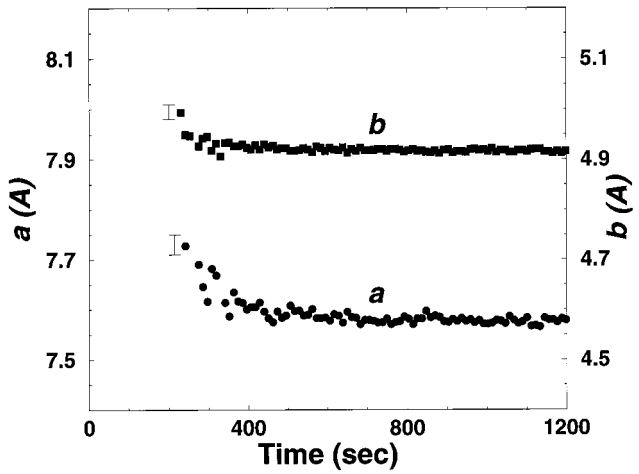

Figure 7. Unit cell quantities from synchrotron WAXS during crystallization of E1 at an average temperature of 114.5 ± 0.5 °C: *a*-axis (●) and *b*-axis (□).

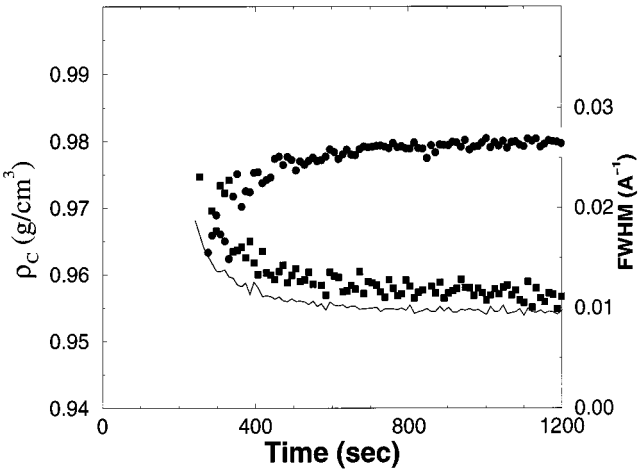

Figure 8. Unit cell quantities from synchrotron WAXS during crystallization of E1 at an average temperature of 114.5 ± 0.5 °C: crystal density ρ_c (●) and full width at half-maximum (FWHM) of the 110 (—) and 200 (■) crystalline reflections.

DSC measurements. During secondary crystallization Q_{SAXS} remains constant while Φ_C further increases (Figure 5). If one assumes that the fraction of spherulites is constant, Φ_c increases as x_{CL} increases (eq 12). Since the long period is relatively constant during this period, one has to conclude that during secondary crystallization, new lamellae are formed in the amorphous regions surrounding lamellar aggregates such that the ratio of the crystal/amorphous thicknesses does not change the average long period significantly. Our Avrami[34] analysis of DSC crystallization exotherms in the temperature range 114−118 °C yields a secondary Avrami constant close to 1.0. This value is to be expected if one assumes that during secondary crystallization process, new crystals are nucleated on preexisting crystals and these crystals are located in the amorphous regions surrounding the lamellar aggregates such as the interlamellar or interfibrillar regions, i.e., one-dimensional growth. Our DSC and SAXS results suggest that the dominant secondary crystallization process is by nucleation on preexisting crystals and these secondary crystals are confined to the amorphous regions surrounding the lamellar aggregates.

In the sample studied, even though molecular weight fractionation can occur in this sample during crystallization as for polydisperse linear polyethylene, we believe that segregation due to the wide distribution in ethylene sequences along each polymer molecule is more important. It is possible that the initial stages of crystallization involves the aggregation of the longest ethylene sequences of a given molecule coalesce with similar segments of adjacent molecules. These aggregates form a spherulitic framework for the subsequent crystallization of shorter ethylene sequences. The evolution of the H_V SALS pattern can be described by an increase in the internal order of the spherulites as crystallization proceeds and/or a process where bundle-like crystals which evolve into sheaves and eventually into complete spherulites by branching or splaying. This morphological interpretation is consistent with previous microscopic studies.[9−17,35,36] For the sample studied, we propose that dominant lamellae are formed by the crystallization of the longest ethylene sequences along the chain while subsidiary lamellae are formed from shorter sequences. For monodiperse and commercial linear polyethylene, secondary crystallization accounts for 5−10% of the crystallinity that develops at moderate to large undercoolings.[3,37] For our sample, the data show that in this case of crystallization at large supercooling, over 30% of the crystallinity develops after the primary crystallization process. At higher temperatures, a larger fraction of the crystallinity develops after the primary process.

At present it is not clear whether the above observations are limited to the specific ethylene copolymer studied. It is hoped that the reported observation will stimulate further crystallization kinetic studies on ethylene copolymers with better characterized composition and structure, in order to establish the generality of the results of the present paper.

Acknowledgment. Synchrotron work was carried out at the SUNY Beamline at the National Synchrotron Light Source, Brookhaven National Laboratory. The authors gratefully acknowledge support of this research by the National Science Foundation, DMR Grant No. 9625485, Materials Research Science and Engineering Center, University of Massachusetts. B.S.H. expresses thanks for the financial support of another NSF grant (DMR 9732653). We would like to thank Dr. Hervé Marand for donating samples provided by Dow Chemical Company and Professor Leo Mandelkern for his many helpful suggestions.

References and Notes

(1) Cronauer, J.; Groth, S.; Zachmann, H. G. Stein, R. S. *J. Mol. Struct.* **1996**, *383*, 19.
(2) Cronauer, J., Dissertation, University of Hamburg, "*Untersuchung der Morphologie und Kristallisation von Polymeren und Polymermischungen unter Anwendung der gleichzeitigen Messung der Röntgenkleinwinkel-, Röntgenweitwinkel-, und Lichtstreuung*," Verlag Shaker: Hamburg, Germany, 1995.
(3) Bark, M.; Zachmann, H. G.; Alamo, R.; Mandelkern, L. *Makromol. Chem.* **1992**, *193*, 2363.
(4) A Song, H. H.; Stein, R. S.; Wu, Q. D.; Ree, M.; Phillips, J. C.; LeGrand, A.; Chu, B. *Macromolecules* **1988**, *21*, 1180.
(5) Song, H. H.; Wu, Q. D.; Chu, B.; Satkowski, M.; Ree, M.; Stein, R. S.; Phillips, J. C. *Macromolecules* **1990**, *23*, 2380.
(6) Hu, S. R.; Kyu, T.; Stein, R. S. *J. Polym. Sci., Polym. Phys. Ed.* **1987**, *25*, 71.
(7) Kyu, T.; Hu, S. R.; Stein, R. S. *J. Polym. Sci., Polym. Phys. Ed.* **1987**, *25*, 89.
(8) Ree, M.; Kyu, T.; Stein, R. S. *J. Polym. Sci., Polymer Physics Ed.* **1987**, *25*, 105.
(9) Bassett, D. C.; Hodge, A. M. *Proc. R. Soc. London, A* **1981**, *377*, 25−37.
(10) Bassett, D. C.; Hodge, A. M. *Proc. R. Soc. London A* **1981**, *377*, 39−60.
(11) Bassett, D. C.; Hodge, A. M. *Proc. R. Soc. London A* **1981**, *377*, 61−71.
(12) Bassett, D. C. *Principles of Polymer Morphology*; Cambridge: Cambridge, England, 1981.
(13) Marand, H. Private communication.
(14) Bensason, S.; Minick, J.; Moet, A.; Chum, S.; Hiltner, A.; Baer, E. *J. Polym. Sci., Part B: Polym. Phys.* **1966**, *34*, 1301−1315.
(15) Kim, Y. S.; Chung, C. I.; Lai, S. Y.; Hyun, K. S. *J. Appl. Polym. Sci.* **1996**, *59*, 125−137.
(16) Alamo, R. G.; Viers, B. D.; Mandelkern, L. *Macromolecules* **1993**, *26*, 5740.
(17) Wunderlich, B. In *Macromolecular Physics, Volume 1: Crystal Structure Morphology, Defects*, Academic: New York, 1973.
(18) Hsiao, B.; Sauer, B. B.; Verma, R. K.; Zachmann, G. H.; Sönke, Seifert.; Chu, B.; Harney, P. *Macromolecules* **1995**, *28*, 6931.
(19) Alexander, L. E. *X-ray Diffraction methods in Polymer Science*; Wiley: New York, 1969.
(20) Ruland, W. *Acta. Crystallogr.* **1961**, *14*, 1180.
(21) Ruland, W. *Polymer* **1964**, *5*, 89; *220*, 19.
(22) Santa Cruz, C.; Stribeck, N.; Zachmann, H. G.; Balta Calleja, F. J. *Macromolecules* **1991**, *24*, 5980.
(23) Hsiao, B. S.; Verma, R. K. *J. Synchrotron Radiat.* **1998**, *5*, 23.
(24) Verma, R.; Marand, H.; Hsiao, B. *Macromolecules* **1996**, *29*, 7767.
(25) Vonk, C, G. *J. Appl. Crystallogr.* **1973**, *6*, 81.
(26) Glatter, O. In *Small Angle X-ray Scattering*; Glatter, O., Kratky, O., Eds.; Academic: London, 1982; Chapter 4.
(27) van Egmond, J. W.; Fuller, G. G. *Macromolecules* **1993**, *26*, 7182.
(28) Stein, R. S.; Keane, J. *J. Polym. Sci.* **1955**, *17*, 21.
(29) Stein, R. S.; Rhodes, M. B. *J. Appl. Phys.* **1960**, *31*, 1873.
(30) Yoon, D. Y.; Stein, R. S. *J. Polym., Sci., Polym. Phys. Ed.* **1974**, *12*, 735.
(31) Koberstein, J. T.; Russel, T.; Stein, R. S. *J. Polym., Sci., Polym. Phys. Ed.* **1979**, *17*, 1719.
(32) Prud'homme, R.; Bourland, L.; Natarajan, R. T.; Stein, R. S. *J. Polym. Sci: Polym. Phys. Ed.* **1974**, *12*, 1955.
(33) Natarajan, R. T.; Prud'homme, R.; Bourland, L.; Stein, R. S. *J. Polym. Sci: Polym. Phys. Ed.* **1974**, *12*, 1955.
(34) Avrami, M. *J. Chem. Phys.* **1939**, *7*, 1103; *J. Chem. Phys.* **1941**, *9*, 177.
(35) Voigt-Martin, I. G.; Fisher, E.; Mandelkern, L. *J. Polym. Sci., Polym. Phys. Ed.* **1980**, *18*, 2347.
(36) Allen, R. C.; Mandelkern, L. *J. Polym. Sci., Polym. Phys. Ed.* **1982**, *20*, 1465.
(37) Hay, J. N.; Mills, P. J. *Polymer* **1982**, *23*, 1380.

MA9810114